

The Effect of Light Nuclei on Chemical Freeze-out Parameters at RHIC Energy

Ning Yu,^{1,2,*} Zuman Zhang,^{1,2} Hongge Xu,^{1,2} and Minxuan Song¹

¹*School of Physics and Mechanical Electrical and Engineering,
Hubei University of Education, Wuhan 430205, China*

²*Institute of Theoretical Physics, Hubei University of Education, Wuhan 430205, China*

(Dated: March 26, 2024)

Abstract

This study examines the chemical freeze-out of hadrons, encompassing light-flavor, strange-flavor, and light nuclei produced in Au+Au collisions at the Relativistic Heavy Ion Collider (RHIC). By conducting a thermal analysis of hadron yields with and without the inclusion of light nuclei yields, we observe a discernible decrease in the chemical freeze-out temperature T_{ch} when light nuclei yields are considered. This suggests that light nuclei formation occurs at a later stage of the system evolution. Furthermore, the T_{ch} associated with strange-flavor particles is found to be approximately 20–30 MeV higher than that for light-flavor particles and light nuclei, hinting at the existence of multiple freeze-out hyper-surfaces for different hadron types in heavy-ion collisions. We present parameterized formulas that describe the energy dependence of T_{ch} and μ_B for four distinct particle sets in central Au+Au collisions. These formulas allow for the selection of appropriate parameters tailored to specific studies, facilitating a more nuanced understanding of the freeze-out process.

PACS numbers: 25.75.Nq, 24.10.Lx, 24.10.Pa

* ning.yuchina@gmail.com

I. INTRODUCTION

Quantum Chromodynamics (QCD) is the fundamental theory of the strong interaction, which describes the interactions between quarks and gluons. One of the major goals of ultra-relativistic nuclear collision is to explore the properties of the QCD phase diagram [1], which shows the possible phases of QCD matter under different temperature and baryon density conditions. According to lattice QCD calculations, a deconfinement transition from hadronic matter to a new state of matter, named quark-gluon plasma (QGP), has been predicted at high temperature and low baryon density [2]. The QGP is a state where quarks and gluons are no longer confined inside hadrons, but can move freely in a hot and dense medium. The existence of QGP has been confirmed by various experimental signatures observed in heavy-ion collisions at ultra-relativistic energies, such as the suppression of high transverse momentum (p_T) hadrons due to jet quenching [3, 4] and the large elliptic flow (v_2) for hadrons due to collective expansion [5–7].

After the discovery of the strongly coupled QGP, efforts have been made to vary the collision energy and to explore the phase structure of the hot and dense QCD matter, which can be represented by the $T - \mu_B$ plane (T : temperature, μ_B : baryon chemical potential) of the QCD phase diagram. One of the most powerful tools to probe the QCD phase diagram is the hadron production, which reflects the thermodynamic conditions of the system at chemical freeze-out. Hadron yields have been measured from AGS to LHC energies and can be well described by a thermal statistical model, assuming that chemical equilibrium is reached [8–11]. The temperature T_{ch} and μ_B at chemical equilibrium, which are also referred to as the “chemical freeze-out” parameters when all hadron abundances are fixed, are determined from a fit to the experimental data.

One of the remarkable findings of the previous studies at LHC energy was that the chemical freeze-out temperature $T_{\text{ch}} = 156.5 \pm 1.5$ MeV obtained from the thermal fit to the hadron and light nuclei yields [11] was consistent with the pseudo-critical temperature $T_c = 154 \pm 9$ MeV obtained from lattice QCD calculations [12] within uncertainties. This suggests that chemical freeze-out occurs close to the phase boundary between QGP and hadronic matter. The data used for the thermal fit were from ALICE Collaboration, which measured not only hadrons but also light nuclei, such as $d(\bar{d})$, ${}^3\text{He}({}^3\overline{\text{He}})$, ${}^4\text{He}({}^4\overline{\text{He}})$, and hyper-triton ${}^3_{\Lambda}\text{H}$ [11]. On the other hand, the chemical freeze-out temperature $T_{\text{ch}} = 167.8 \pm 4.2$ MeV

extracted by thermal fit at RHIC top energy was higher than the value at LHC and T_c [9], while only hadron yields are included in the fitting. These differences between RHIC and LHC thermal analyses might stem from the light nuclei production, which could modify the chemical freeze-out conditions.

In relativistic heavy-ion collisions, the underlying mechanisms for the production of light nuclei are not well understood [13–17]. One possible scenario is that light nuclei are formed by the coalescence of nucleons in the final state [18, 19]. Another possible scenario is that light nuclei are produced by the thermal model [11, 20, 21], in which protons, neutrons, and light nuclei reach chemical equilibrium. From the coalescence picture, the effective temperature of the final state is lower than the temperature at chemical freeze-out. In Ref. [15], it is shown that the (anti-)deuteron yield is nearly constant during the evolution, if it is thermally initialized. The (anti-)deuteron can be both destroyed and created by the reaction $\pi d \leftrightarrow \pi pn$, which means that the thermal and coalescence models with different assumptions can give similar (anti-)deuteron yields.

To investigate the differences of T_{ch} between RHIC and LHC, we use a statistic thermal model to analyze the hadron [9], (anti-)deuteron [14] and triton [22] yield at RHIC energy. We compare the extracted freeze-out parameters with different sets of particle yields and discuss the underlying physics of the production of strange, light flavor, and light nuclei.

II. STATISTICAL THERMAL MODEL

The chemical properties of the bulk particle production can be treated in the framework of the thermal statistical models, using the Thermal-FIST package [23]. It is based on the hadron resonance gas (HRG) model and allows one to calculate thermodynamic features and fluctuation observables with arbitrary attractive and repulsive interactions between each type of hadron species. In the grand-canonical ensemble (GCE), the conserved charges, such as baryonic number B , electric charge Q , strangeness S , and charm C , are conserved on average. For the chemical equilibrium case these average values are regulated by their corresponding chemical potentials, $\mu_B, \mu_S, \mu_Q, \mu_C$. The chemical potential μ_i of hadron species i is determined as

$$\mu_i = B_i \mu_B + S_i \mu_S + Q_i \mu_Q + C_i \mu_C. \quad (1)$$

TABLE I. Particle Set in Our Fitting.

Particle Set	Particle list
I	$\pi^\pm, K^\pm, p(\bar{p}), \Lambda(\bar{\Lambda}), \Xi^-(\bar{\Xi}^+)$
II	$\pi^\pm, K^\pm, p(\bar{p}), \Lambda(\bar{\Lambda}), \Xi^-(\bar{\Xi}^+), d(\bar{d})$
III	$\pi^\pm, K^\pm, p(\bar{p}), \Lambda(\bar{\Lambda}), \Xi^-(\bar{\Xi}^+), d(\bar{d}), t$
IV	$p(\bar{p}), d(\bar{d}), t$

The particle density can be parameterized by

$$\frac{N_i(T, \mu_i)}{V} = g_i \int \frac{d^3p}{(2\pi)^3} \left[\gamma_s^{-|S'_i|} \exp\left(\frac{E_i - \mu_i}{T_{ch}}\right) + \eta_i \right]^{-1}, \quad (2)$$

where g_i , $E_i = \sqrt{p^2 + m_i^2}$ and m_i are, respectively, the spin degeneracy factor, energy and mass of hadron species i . η_i equals +1 for fermions, -1 for bosons, and 0 for the Boltzmann approximation. γ_s is the strangeness under-saturation factor that regulates the deviation from chemical equilibrium of the strange quarks. S'_i is the number of valence strange and anti-strange quarks in particle i .

By collecting the invariant yields of hadrons, (anti-)deuterons, and tritons from Au+Au collisions at RHIC [9, 14, 22, 24], four different sets of particle yields are used in the fit. The first set is the same as Ref. [9], which include the yields of π^\pm , K^\pm , $p(\bar{p})$, $\Lambda(\bar{\Lambda})$, and $\Xi^-(\bar{\Xi}^+)$. The (anti-)deuterons yields are included in the second particle set. In particle set III, the triton yields are included. In the fourth particle set, we exclude all the mesons and strange hadrons, which means only $p(\bar{p})$, $d(\bar{d})$, and t are included. The four particle sets are listed in Table I.

In our fitting, we use the GCE. The quantum statistic is considered for mesons only, that is $\eta_i = -1$ for π^\pm and K^\pm , while $\eta_i = 0$ for other particles. The finite widths of resonances with a Breit-Wigner form mass distribution are taken into account in our fitting [25]. The μ_Q and μ_S are determined in a unique way in order to satisfy two conservation laws given by the initial conditions: the electric-to-baryon charge ratio of $Q/B = 0.4$ for Au+Au collisions, and the vanishing net strangeness $S = 0$. Therefore, we are left with only four parameters that need to be fitted. Those are the freeze-out temperature T_{ch} , the baryon chemical potential μ_B , the strangeness under-saturation factor γ_s and the fireball radius (the fireball volume is $V = 4/3\pi R^3$).

III. RESULTS

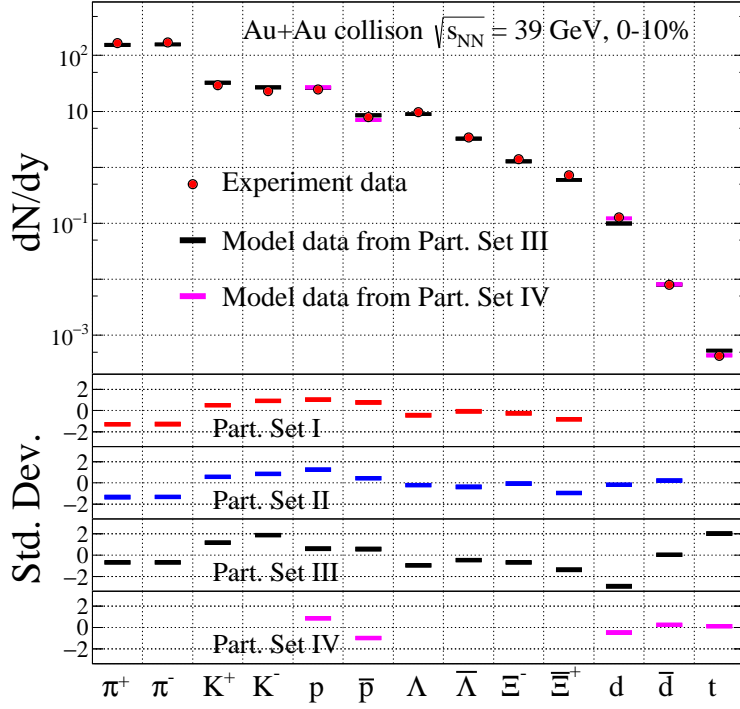


FIG. 1. Particle abundance and prediction of the statistical hadronization model. Upper panel: dN/dy values (red circles) from different hadrons and nuclei, measured at mid-rapidity, are compared with the thermal fit (magenta and blue bars). The data are from the STAR Collaboration for 0 – 10% Au+Au collisions at $\sqrt{s_{\text{NN}}} = 200$ GeV. Lower panel shows the standard deviations σ between thermal fit and experimental data.

Figure 1 presents the results from GCE thermal fit by different particle sets and the standard deviations, σ , between the model and the data measured by STAR experiment for 0-10% Au+Au collisions at $\sqrt{s_{\text{NN}}} = 39$ GeV. It can be observed that the deviations for π and Ξ^- do not change significantly when the yield of (anti-)deuterons is included in the fit. Interestingly, the fit performance for p and \bar{p} improves when the yield of (anti-)deuterons is included in the fit, which might suggest that the thermal (anti-)deuterons are produced at the stage when protons achieve chemical freeze-out.

Figure 2 depicts the centrality dependence of chemical freeze-out parameters T_{ch} and μ_B , as determined by the thermal fit of four distinct particle yield sets for Au+Au collisions at $\sqrt{s_{\text{NN}}} = 200$ GeV. In the upper panel of figure 2, it can be observed that as centrality

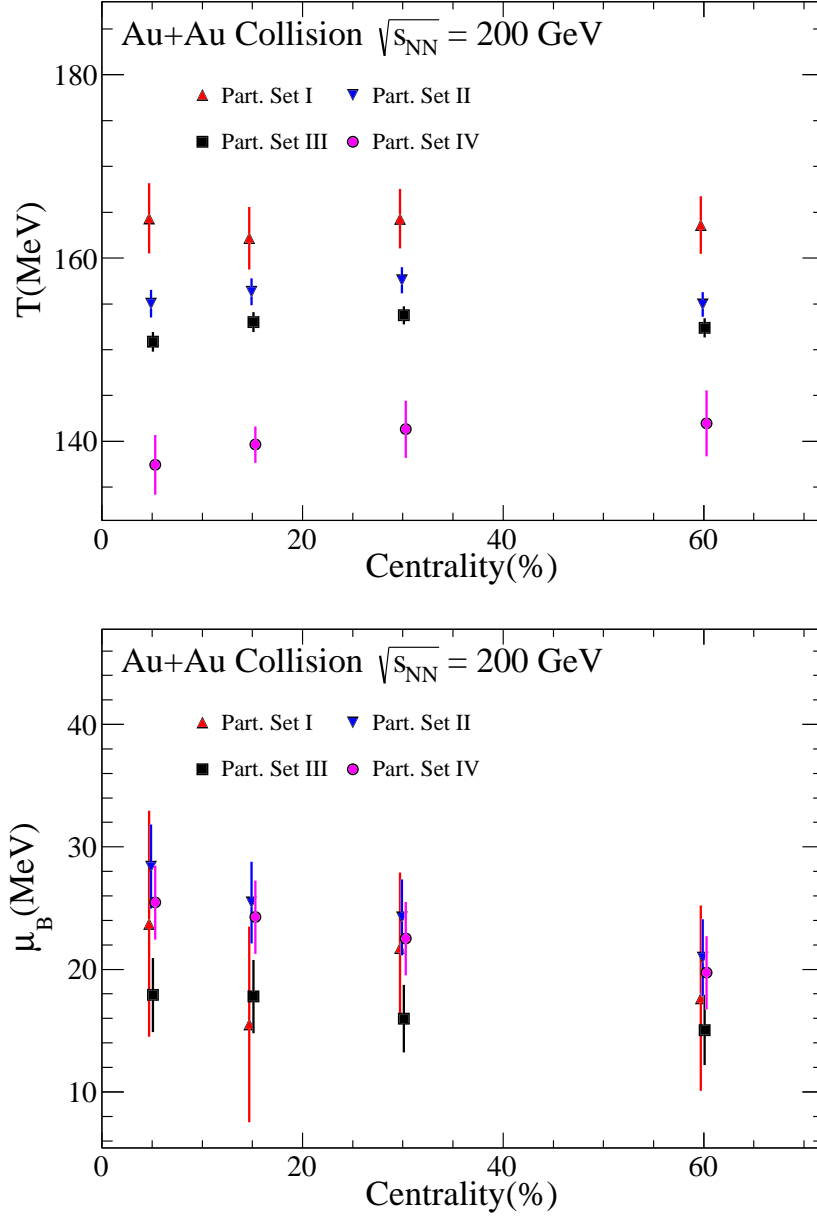


FIG. 2. Centrality dependence of chemical freeze-out parameters T_{ch} (upper panel) and μ_B (bottom panel). The results are obtained from the thermal fit by four different particle sets for 0 – 10% Au+Au collisions at $\sqrt{s_{\text{NN}}} = 200$ GeV.

increases, indicating a shift from central to peripheral collisions, the T_{ch} for all particle sets exhibits a consistent trend, remaining independent of centrality. A significant observation from the upper panel of figure 2 is that the value of T_{ch} derived from the thermal fit varies depending on the specific particles included in each set. When the yield of (anti-)deuterons

is included in the fit, the T_{ch} decreases from approximately 165 MeV (Particle Set I) to 155 MeV (Particle Set II). The inclusion of tritons in the fit further reduces the fitted T_{ch} to 150 MeV (Particle Set III). Most notably, when the fit is performed using only the yields of light nuclei and their constituent nucleons (protons), the T_{ch} drops to as low as 140 MeV (Particle Set IV). The significant decrease in temperature with the inclusion of light nuclei suggests that light nuclei may undergo chemical freeze-out at a later stage compared to other particles. This could potentially be attributed to the different production mechanisms of light nuclei in heavy-ion collisions.

In the lower panel of figure 2, we observe the behavior of the baryon chemical potential μ_B across different centralities. As centrality increases, μ_B appears to decrease for all particle sets. The baryon chemical potential μ_B is related to the net-baryon density [26]. This behavior suggests that as collisions shift from central to peripheral, the net baryon density of the system at the time of chemical freeze-out decreases. Furthermore, unlike the T_{ch} , the value of μ_B derived from different particle sets is consistent within error of our measurements. This consistency could be attributed to the relatively small yields of light nuclei compared to other particles, resulting in a minor impact on the net baryon density and, consequently, a smaller effect on μ_B .

The freeze-out temperature T_{ch} versus the baryon chemical potential μ_B from the thermal fit by four different particle sets from Au+Au collisions at $\sqrt{s_{\text{NN}}} = 200, 39, 19.6, 11.5, \text{ and } 7.7$ GeV are depicted in Figure 3. The symbols from 14.5, 27, and 62.4 GeV have been omitted for clarity. On the graph, five different elliptical dashed lines label the results corresponding to various energies. The figure illustrates the dependence of freeze-out temperature T_{ch} on both the collision energies and particle sets. For each specific particle set, a gradual decrease in T_{ch} is observed as the collision energy diminishes. Interestingly, this energy dependence vanished with the error when considering Particle Set IV, which includes only protons, deuterons and tritons. All collision energy fits converge around a T_{ch} of approximately 140 MeV. This convergence suggests that the process producing light nuclei via nucleon coalescence occurs at an approximate temperature of 140 MeV, or that light nuclei freeze-out at lower temperatures compared to other hadrons which freeze-out at higher temperatures. This observation potentially accounts for why the freeze-out temperatures derived from the top energy at RHIC [9] are higher than those obtained from LHC results [11], as multiple light nuclei yields were incorporated in the LHC fits. For the baryon chemical potential

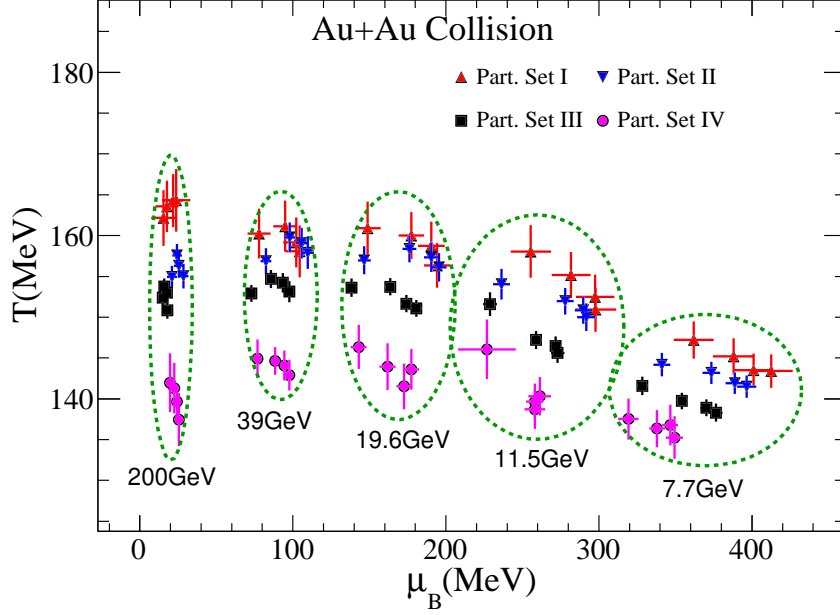


FIG. 3. Energy dependence of chemical freeze-out parameters T_{ch} and μ_B . The results are derived from the thermal fit by four different Particle Sets from Au+Au collisions at $\sqrt{s_{\text{NN}}} = 200, 39, 19.6, 11.5$, and 7.7 GeV. Elliptical dashed lines represent the results corresponding to different collision energies.

μ_B , a distinct energy dependence is observed. With decreasing collision energy, the yield of anti-baryons diminishes while the net baryon density increases, resulting in a rise in μ_B . Analogous to the findings presented in Figure 1, various Particle Sets give similar μ_B values.

Formulas for the parameterization of the chemical freezing parameter T_{ch} and μ_B , using collision energy $\sqrt{s_{\text{NN}}}$ as a variable, are provided in reference [11] with the following expressions:

$$T_{\text{ch}} = T_{\text{ch}}^{\text{lim}} \frac{1}{1 + \exp\{a - \ln[\sqrt{s_{\text{NN}}}(\text{GeV})]/b\}} \quad (3)$$

$$\mu_B = \frac{c}{1 + d\sqrt{s_{\text{NN}}}(\text{GeV})}$$

These parameterized equations use experimental fit data from STAR and LHC. The chemical freeze-out parameters for STAR and LHC were fitted with different particle sets, as previously discussed. From the previous discussion it is evident that incorporating light nuclei in the fitting process yields varied chemical freeze-out temperatures. Therefore, it is essential to parameterize the chemical freezing parameters derived from different particle sets. Figure 4 presents the results of parameterized chemical freeze-out parameters, obtained

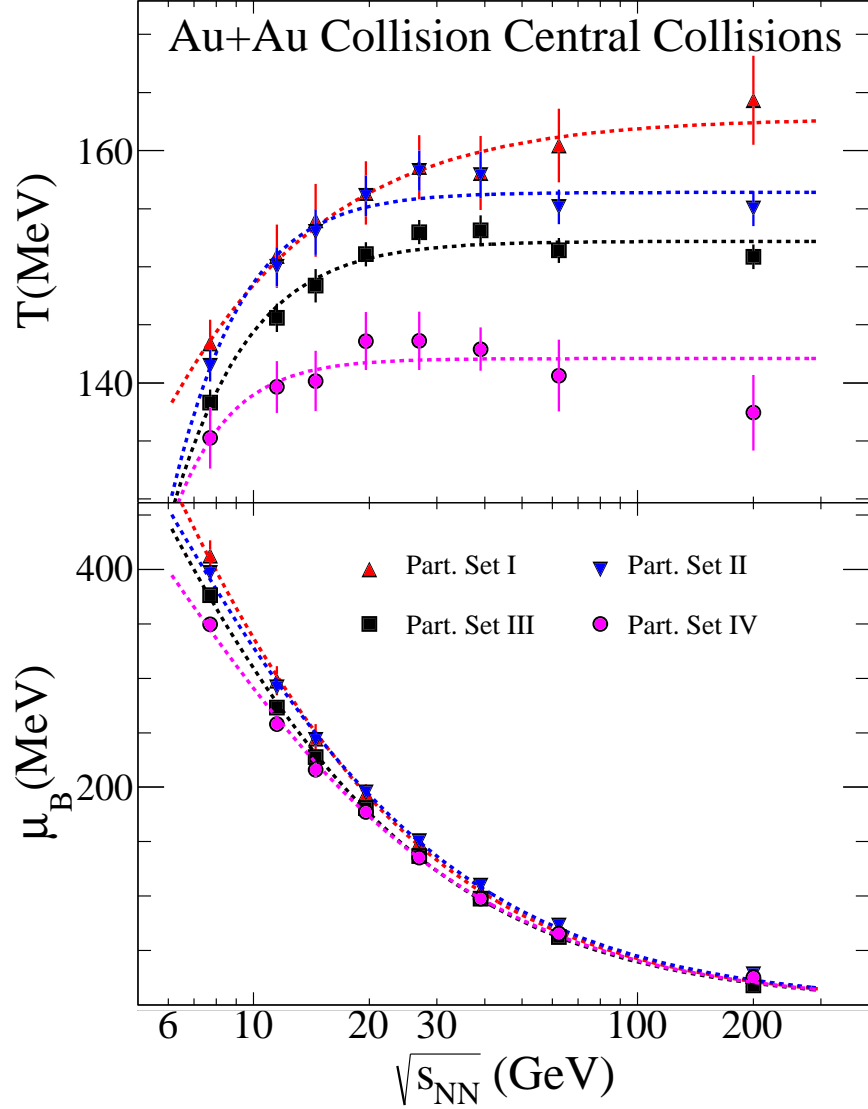


FIG. 4. Energy dependence of temperature and baryon chemical potential from Au + Au collisions at $\sqrt{s_{\text{NN}}} = 200, 39, 19.6, 11.5,$ and 7.7 GeV for four different Particle Sets. The lines are parametrizations for T_{ch} and μ_B .

through fits with various particle sets in Au+Au central collision. The parameters are given in Table II.

It can be seen that different particle sets yield different $T_{\text{ch}}^{\text{lim}}$ values, and as more light nuclei are added to the fit, the $T_{\text{ch}}^{\text{lim}}$ obtained becomes smaller. If the fit contains only proton and light nuclei, the $T_{\text{ch}}^{\text{lim}}$ becomes even smaller, only around 142 MeV.

By employing thermodynamic statistical model fitting, a pair of (T_{ch}, μ_B) values can be obtained for the hadronic yield at each collision energy. In Figure 5, these points are plotted

TABLE II. The parameters in energy-dependent T_{ch} and μ_B

Particle Set	$T_{\text{ch}}^{\text{lim}}(\text{MeV})$	a	b	$c(\text{MeV})$	d
Ref. [11]	158.4 ± 1.4	2.60	0.45	1307	0.286
I	162.8 ± 3.8	0.50	0.81	1442 ± 304	0.328
II	156.4 ± 0.9	3.36	0.37	1089 ± 83	0.232
III	152.2 ± 0.6	2.75	0.41	1261 ± 90	0.308
IV	142.1 ± 1.3	3.59	0.31	905 ± 62	0.211

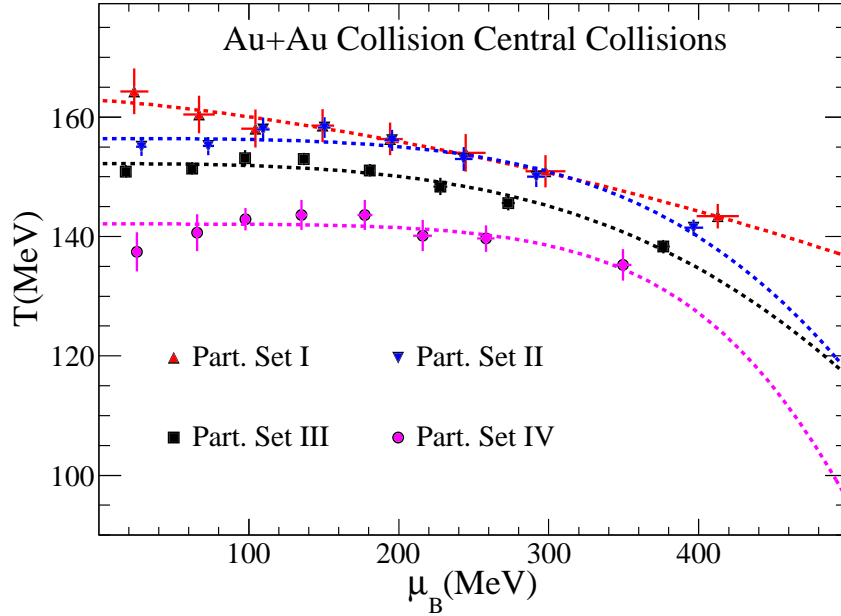


FIG. 5. Chemical freeze-out parameters T_{ch} versus baryon chemical potential μ_B from Au + Au collisions at $\sqrt{s_{\text{NN}}} = 200, 39, 19.6, 11.5,$ and 7.7 GeV for four different Particle Sets. The lines are from Eq. 3

in a two-dimensional phase diagram of T_{ch} versus μ_B , which can be used to characterize the phase boundary between hadronic matter and the QGP. It is observed that there are several distinct boundaries for different particle sets. This might suggest that different particles are produced at different freeze-out hyper-surfaces, particularly for light nuclei whose freeze-out hyper-surface corresponds to a lower temperature. It is well established that the fireballs of dense matter produced in nuclear-nuclear collisions cool, expand, and decomposes into the final-state hadrons over time. Strange quarks are known to reach chemical equilibrium

before they coalesce into hadrons at a temperature higher than 160 MeV [27]. Strangeness hadrons, especially multi-strange hadrons are expected to have relatively smaller hadronic interaction cross sections than light hadrons [28, 29]. Consequently, the primary yield of strangeness particles will experience little change from the stage of phase transition due to hadronic interaction. As a result, they can carry the temperature information from the quarks' chemical equilibrium, which is higher than the temperature at which light hadron chemical freeze-out occurs, and display a clear sequence of chemical freeze-out during the system evolution. This finding is consistent with our analysis using Particle Set I, which includes most of the strange hadrons detectable in experiments and their daughter particles π^\pm . For light nuclei and light hadrons, their yields change as the system evolves, indicating that they reach chemical equilibrium much later, i.e., they freeze out of the system at lower temperatures. This explains why Particle Set I yields a relatively low-temperature freeze-out hyper-surface.

IV. SUMMARY

Thermodynamic statistical model fitting enables the precise determination of chemical freeze-out parameters T_{ch} and μ_B during relativistic heavy-ion collisions. These parameters provide crucial insights into the phase transition from QGP to hadronic matter. In this study, by fitting experimental data on particle yields at mid-rapidity from RHIC-STAR at various collision energies, we have elucidated the centrality and energy dependence of the chemical freeze-out parameters for different particle sets. Parameterized formulas depicting the variation of T_{ch} and μ_B with collision energy $\sqrt{s_{\text{NN}}}$ for different particle sets have been presented. The parameters within these formulas suggest the possibility of distinct freeze-out hyper-surfaces for different particles. Specifically, hadrons containing strange quarks exhibit freeze-out hyper-surfaces at relatively higher temperatures, while those composed solely of light quarks, as well as light nuclei, show freeze-out hyper-surfaces at a 20 – 30 MeV lower temperatures. This indicates that light nuclei freeze out later during the system evolution.

This nuanced understanding of the freeze-out process provides valuable insights into the complex dynamics of nuclear-nuclear collisions and the conditions that lead to the formation of different particle species. It emphasizes the necessity of taking into account the distinct

freeze-out scenarios for different particles, especially light nuclei. The findings align with experimental data and contribute to the broader goal of mapping the QGP phase diagram, a fundamental aspect of high-energy nuclear physics research.

-
- [1] P. Braun-Munzinger and J. Wambach, *Rev. Mod. Phys.* **81**, 1031 (2009).
 - [2] F. Karsch, *Prog. Part. Nucl. Phys.* **62**, 503 (2009).
 - [3] L. Adamczyk *et al.* (STAR Collaboration), *Phys. Rev. Lett.* **121**, 032301 (2018).
 - [4] J. Adams *et al.* (STAR Collaboration), *Nucl. Phys. A* **757**, 102 (2005).
 - [5] K. Adcox *et al.* (PHENIX Collaboration), *Nucl. Phys. A* **757**, 184 (2005).
 - [6] I. Arsene *et al.* (BRAHMS Collaboration), *Nucl. Phys. A* **757**, 1 (2005).
 - [7] B. B. Back *et al.* (PHOBOS Collaboration), *Nucl. Phys. A* **757**, 28 (2005).
 - [8] P. Braun-Munzinger, J. Stachel, J. P. Wessels, and N. Xu, *Phys. Lett. B* **365**, 1 (1996).
 - [9] L. Adamczyk *et al.* (STAR Collaboration), *Phys. Rev. C* **96**, 044904 (2017).
 - [10] A. Andronic, P. Braun-Munzinger, and J. Stachel, *Phys. Lett. B* **673**, 142 (2009).
 - [11] A. Andronic, P. Braun-Munzinger, K. Redlich, and J. Stachel, *Nature* **561**, 321 (2018).
 - [12] S. Borsányi, Z. Fodor, C. Hoelbling, S. D. Katz, S. Krieg, C. Ratti, and K. K. Szabó, *J. High Energy Phys.* **2010**, 073 (2010).
 - [13] B. Monreal, W. J. Llope, R. Mattiello, S. Y. Panitkin, H. Sorge, and N. Xu, *Phys. Rev. C* **60**, 051902 (1999).
 - [14] J. Adam *et al.* (STAR Collaboration), *Phys. Rev. C* **99**, 064905 (2019).
 - [15] D. Oliinychenko, L.-G. Pang, H. Elfner, and V. Koch, *Phys. Rev. C* **99**, 044907 (2019).
 - [16] J. Adam *et al.* (ALICE Collaboration), *Phys. Rev. C* **93**, 024917 (2016).
 - [17] J. H. Chen, D. Keane, Y. G. Ma, A. H. Tang, and Z. B. Xu, *Phys. Rep.* **760**, 1 (2018).
 - [18] H. H. Gutbrod, A. Sandoval, P. J. Johansen, A. M. Poskanzer, J. Gosset, W. G. Meyer, G. D. Westfall, and R. Stock, *Phys. Rev. Lett.* **37**, 667 (1976).
 - [19] R. Scheibl and U. Heinz, *Phys. Rev. C* **59**, 1585 (1999).
 - [20] J. Cleymans, S. Kabana, I. Kraus, H. Oeschler, K. Redlich, and N. Sharma, *Phys. Rev. C* **84**, 054916 (2011).
 - [21] A. Andronic, P. Braun-Munzinger, J. Stachel, and H. Stöcker, *Phys. Lett. B* **697**, 203 (2011).
 - [22] M. I. Abdulhamid *et al.* (STAR Collaboration), *Phys. Rev. Lett.* **130**, 202301 (2023).

- [23] V. Vovchenko and H. Stoecker, Comput. Phys. Commun. **244**, 295 (2019).
- [24] S. S. Adler *et al.* (PHENIX Collaboration), Phys. Rev. C **69**, 034909 (2004).
- [25] V. Vovchenko, M. I. Gorenstein, and H. Stoecker, Phys. Rev. C **98**, 034906 (2018).
- [26] N. Yu, F. Liu, and K. Wu, Phys. Rev. C **90**, 024913 (2014).
- [27] J. Rafelski and B. Muller, Phys. Rev. Lett. **48**, 1066 (1982).
- [28] H. van Hecke, H. Sorge, and N. Xu, Phys. Rev. Lett. **81**, 5764 (1998).
- [29] A. Shor, Phys. Rev. Lett. **54**, 1122 (1985).